

Effects of Slot Location on Flow and Heat Transfer in a Latticework Cooling Channel: An MRV Experiment and Numerical Study

Y. X. Jia, H. R. Shen, W. Li, J. M. Wu*

State Key Laboratory for Strength and Vibration of Mechanical Structures
School of Aerospace Engineering, Xi'an Jiaotong University
Xi'an, Shaanxi, China

Abstract

The cooling efficiency and structural reliability of gas turbine engine blades are highly dependent on high-fidelity internal cooling configurations, particularly in the highly constrained trailing edge regions. This study proposes a targeted slotting strategy to optimize the trade-off between heat transfer enhancement and aerodynamic penalty in a rectangular latticework cooling channel. Four geometric configurations—including a baseline unslotted channel (Case 0), an impingement-zone slotted channel (Case 1), a turning-zone slotted channel (Case 2), and a simultaneous dual-slotted channel (Case 3)—are systematically investigated. Three-dimensional full-field velocity distributions are non-intrusively captured at a bulk Reynolds number of 10,000 using Magnetic Resonance Velocimetry (MRV) on a clinical 3.0T MRI scanner. Conjugate heat transfer simulations are concurrently performed over a wider operating range (Re = 10,000 to 25,000) and validated against the MRV experimental benchmark. The results indicate that while the impingement slot (Case 1) disrupts the macro-scale swirl intensity within the sub-channel core, it effectively mitigates localized wake separation. Conversely, the turning slot (Case 2) acts as a fluidic accelerator that strengthens the core vortex rotational momentum but fails to suppress the upstream rib separation bubble. Crucially, the dual-slotted configuration (Case 3) exhibits a synergistic aerodynamic intervention, leveraging a self-governing suction-and-blowing mechanism to eliminate cumulative downstream flow stagnation zones near the endwall (sub-channels C7 and C8). Consequently, Case 3 substantially recovers the effective flow capacity, yielding a significantly reduced friction factor ratio (f/f_0) and a superior thermal performance factor (TPF) that increases monotonically with rising Re. This targeted dual-slot approach demonstrates exceptional aerothermal viability for advanced turbomachinery cooling design.

Keywords: Latticework cooling channel; Slot location; flow characteristic; Heat transfer; MRV;

1. Introduction

The cooling efficiency of gas turbine engines is intrinsically linked to the turbine inlet temperature (TIT). It is well-established that increasing the TIT significantly improves thrust and power generation efficiency; however, modern operating temperatures have far exceeded the melting limits of superalloy materials [1]. Consequently, the development of highly efficient internal cooling structures is critical to ensuring the survivability of turbine components, particularly in the trailing edge region where heat flux is extreme and space is constrained [2].

Among various cooling topologies, lattice cooling structures have attracted considerable attention due to their superior heat transfer performance and structural robustness [3]. Unlike conventional ribbed channels, lattice structures are characterized by a network of intersecting sub-channels formed by inclined ribs. This unique geometry forces the coolant to undergo continuous 180-degree turns as it traverses the structure, generating strong secondary flows and longitudinal vortices that disrupt thermal boundary layers [4, 5]. Previous studies by Bunker [6] and Saha et al. [7] have demonstrated that these flow features allow lattice structures to achieve heat transfer coefficients significantly higher than those of traditional pin-fin arrays.

https://doi.org/10.71945/icas2026_0545

However, the complex flow topology that enhances heat transfer also imposes a severe aerodynamic penalty. As the coolant navigates the sharp turns within the lattice sub-channels, it undergoes intense flow reversal and impingement against the channel sidewalls. This phenomenon results in significant flow separation and high local pressure losses, which can detrimentally affect the overall cooling efficiency [8, 9]. To mitigate this, researchers have investigated various geometric modifications. One such approach is the introduction of slots or gaps in the rib structures. For instance, Choi et al. [10] and Du et al. [11] indicated that discontinuous ribs could alter the flow trajectory and reduce pressure drop. Yet, existing slotting strategies often lack specificity regarding the local flow physics at the turning points.

The critical issue lies in the non-uniform distribution of impact forces along the channel walls. The flow impingement is most intense at specific sidewall locations near the turning regions. Therefore, a targeted approach is required. This study proposes a novel slotting configuration specifically designed for the sidewall regions where the fluid impact force is maximized. The core idea is to introduce slots at these high-impingement zones to alleviate flow blockage and reduce resistance, while simultaneously guiding the fluid to enhance mixing. By focusing on these critical locations, we aim to optimize the trade-off between thermal performance and pressure loss.

2. Experiment Setup and Measurement Methods

To validate the proposed slotting strategy and understand the underlying flow physics, it is imperative to establish a clear "cause-and-effect" relationship between the geometric modifications and the 3D flow field evolution. This presents a significant challenge for experimental fluid mechanics. Traditional optical measurement techniques, such as Particle Image Velocimetry (PIV) and Laser Doppler Velocimetry (LDV), are severely restricted in these opaque, complex internal passages due to the lack of optical access [12, 13]. While CFD is a powerful tool, it often relies on turbulence models that struggle to accurately predict the complex separation and reattachment phenomena prevalent in lattice geometries without rigorous experimental validation [14, 15]. Magnetic Resonance Velocimetry (MRV) offers a transformative solution to these challenges. Based on the principles of Nuclear Magnetic Resonance (NMR), MRV is capable of non-intrusively measuring the full-field 3D velocity distribution within opaque geometries, bypassing the optical limitations of traditional methods [16, 17]. Unlike point-wise or planar measurements, MRV provides a comprehensive volumetric dataset that is essential for capturing the topology of complex vortices and flow separations in three dimensions [18]. In recent years, MRV has matured into a benchmark experimental technique for turbomachinery flows. Elkins et al. [18] demonstrated the capability of 4D-MRV to measure turbulent pipe flows with high accuracy, validating its ability to resolve Reynolds stresses. In the context of turbine cooling, Benson et al. [19] utilized MRV to study film cooling flows, while Tsuru et al. [5] successfully applied it to visualize the complex 3D flow structures in lattice channels, validating the existence of inter-layer momentum exchange. Furthermore, Duan et al. [20] and Zhang et al. [21] have utilized MRV to validate CFD models for double-wall cooling configurations, proving that MRV data can serve as a "ground truth" for turbulence model assessment. The high-fidelity data obtained from MRV allows for detailed topological analysis of streamlines, vorticity, and vortex-core structures, which are otherwise impossible to obtain in such complex, enclosed geometries [16, 17, 20].

2.1 Experimental Methodology and Apparatus

The three-dimensional full-field velocity measurements were conducted via MRV using a clinical 3.0T MRI scanner (Siemens MAGNETOM Spectra) at Xi'an Jiaotong University. As shown in Fig. 1, the experimental flow loop is a closed circuit driven by a centrifugal pump. To avoid electromagnetic interference, all metallic components—including the pump, water tank, control valves, and flow meters—were positioned outside the MRI shielded room, and the fluid was delivered to the scanner bore via non-magnetic PVC piping.

Deionized water at 20°C (kinematic viscosity v = 1.003 x 10^-6 m^2/s) was used as the working fluid, mixed with 0.06 mol/L $CuSO_4$ to enhance the signal-to-noise ratio (SNR). The test section is a straight rectangular duct with a cross-section of 100 mm x 25 mm (aspect ratio AR = 4:1) and a hydraulic diameter (D_h) of 40 mm. The flow rate was regulated to maintain a steady bulk Reynolds number of Re = 10000, corresponding to a bulk mean velocity of 0.25 m/s.

A three-directional velocity-encoded phase-contrast sequence was executed. The velocity encoding (Venc) limit was set to 2.0 m/s in all three orthogonal directions to prevent phase aliasing. The sequence was configured with an echo time (TE) of 5.9 ms and a repetition time (TR) of 120 ms. The data were acquired over a 448 x 224 x 36 spatial matrix, yielding a spatial resolution (voxel size) of 0.67 mm x 0.67 mm x 1.0 mm.

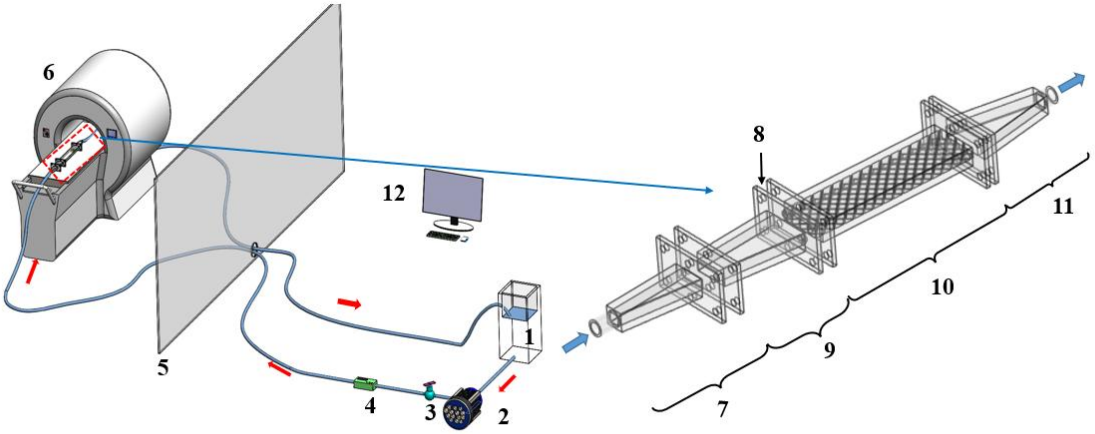


Figure 1 – Schematic diagram of the experimental flow loop system

2.2 Test Model and Structural Configurations

The experimental model consists of a simplified rectangular latticework cooling channel, as illustrated in Fig. 2. The channel features a total width (W) of 100 mm, a height (H) of 25 mm, and an interlocking core length (L) of 208 mm, with the positive x-axis aligning with the mainstream flow direction. Inside the core section, the intersecting ribs form parallel sub-channels with a width (W_p) of 25 mm and an individual rib width (W_r) of 3 mm. The near-wall zones where the fluid undergoes sharp turning are designated as c1 through c8.

To alleviate localized flow blockage near the side walls, slots with a constant width (W_s) of 2 mm are introduced. Based on the local flow kinematics, these near-wall zones are divided into the "turning region" (the upstream fluid layer that the coolant departs from during redirection) and the "impingement region" (the downstream fluid layer that the coolant enters and impinges upon). To investigate the effects of slot locations, four geometric configurations were established:

- Case 0: The baseline channel without slots.
- Case 1: Slotted exclusively in the impingement regions.
- Case 2: Slotted exclusively in the turning regions.
- Case 3: Concurrently slotted in both the impingement and turning regions.

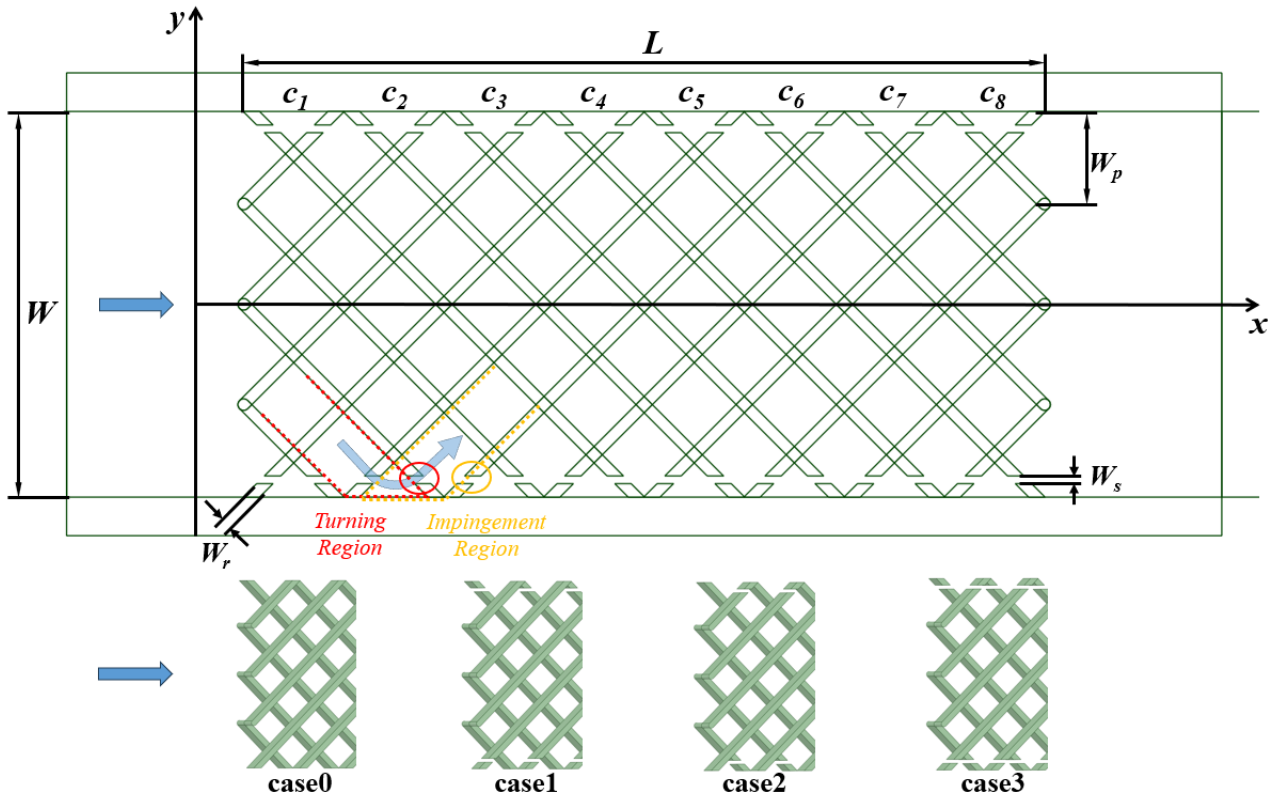


Figure 2 – Schematic diagrams and geometric parameters of the latticework cooling channels for the test cases

3. Numerical Setup

3.1 Governing Equations and Boundary Conditions

The governing equations of turbulent air flow and heat transfer and solid heat conduction used in this study follow the work of Jin et al.[22]. To thoroughly evaluate the convective heat transfer and fluid flow characteristics of the four distinct structural configurations, three-dimensional conjugate heat transfer simulations were performed. Building upon the baseline experimental flow measurements, the numerical analysis was extended to investigate the thermal performance under medium-temperature conditions using air as the working fluid across a wide operating range. The established computational domain and its corresponding boundary conditions are schematically illustrated in Fig. 3.

At the channel inlet, a uniform velocity profile was specified to investigate four distinct Reynolds numbers: Re = 10,000, 15,000, 20,000, and 25,000, based on the characteristic hydraulic diameter (D_h) of 0.04 m. The inlet temperature of the coolant air was maintained at a constant value of Tin = 339 K. A pressure outlet boundary condition with zero gauge pressure was implemented at the channel exit. To simulate the thermal load within the internal cooling passage, a uniform and constant heat flux of q = 15,000 W/m² was applied to the active heating surface of the lattice core region. Thermal energy is transferred from the solid domain to the fluid domain via conjugate heat transfer through a high-temperature superalloy substrate. Accordingly, the fluid-solid interfaces were designated as coupled walls to ensure the continuity of both local temperature and heat flux vectors. All remaining external solid boundaries of the computational domain were defined as adiabatic, no-slip walls to eliminate extraneous thermal losses and isolate the geometric effects on the cooling performance.

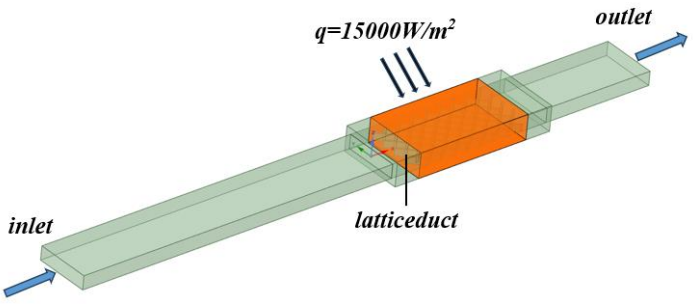


Figure 3 – Schematic of the computational domain and boundary conditions

3.2 Mesh Generation and Grid Independence Verification

In this study, three-dimensional mesh generation was executed using the ANSYS Fluent Meshing platform. To accurately resolve the extremely thin viscous sublayer and comply with the stringent grid requirements of the Enhanced Wall Treatment used in the Realizable k-ε model, the dimensionless wall distance of the first grid layer was strictly controlled to ensure that the wall y+ value was approximately equal to unity (y+ $\approx$ 1) across all solid boundaries. The fluid domain was discretized utilizing the advanced Poly-Hexcore meshing scheme. To faithfully capture the steep velocity and thermal gradients inherent to the near-wall flow, five prism boundary layers with a smooth growth rate were extruded from the fluid-solid interfaces, as schematically illustrated in Fig. 4.

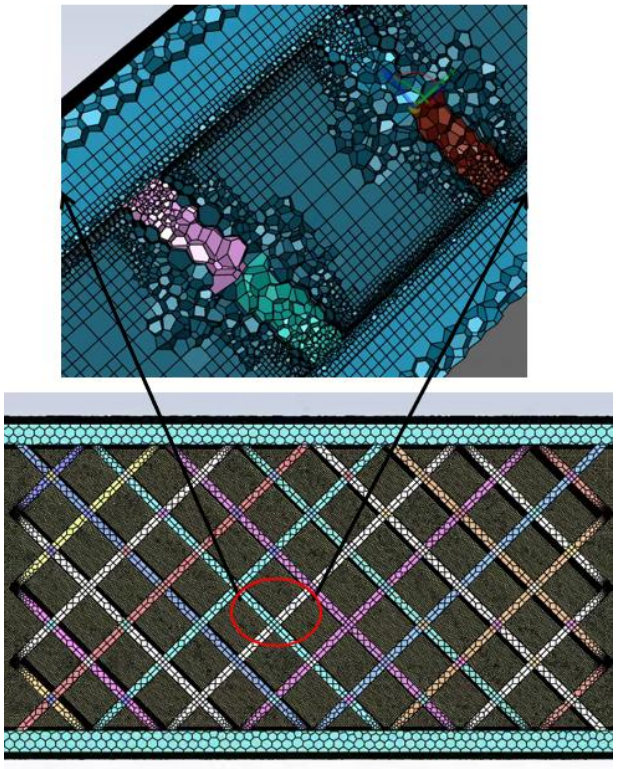


Figure 4 – Local mesh view showing the Poly-Hexcore topology and 5-layer prism boundary layers

To systematically eliminate the influence of grid resolution on the fidelity of the numerical solutions, a rigorous grid independence study was performed. Three sets of meshes with progressively increasing spatial resolutions were established, featuring total cell counts of 2.56 million, 3.07 million, and 3.81 million, respectively. Figure 5 depicts the comparative evaluation of the overall channel pressure drop and targeted flow parameters across the three grid level. The validation results indicate that the discrepancy in the monitored flow features and pressure drop between the 3.07 million mesh and the finest 3.81 million mesh is negligibly small (typically within 1%), demonstrating that asymptotic grid convergence had been successfully achieved. Consequently, by judiciously

balancing the trade-offs between computational cost and numerical accuracy, the mesh configuration with 3.07 million cells was selected as the baseline grid density for all subsequent numerical investigations across the four structural variations.

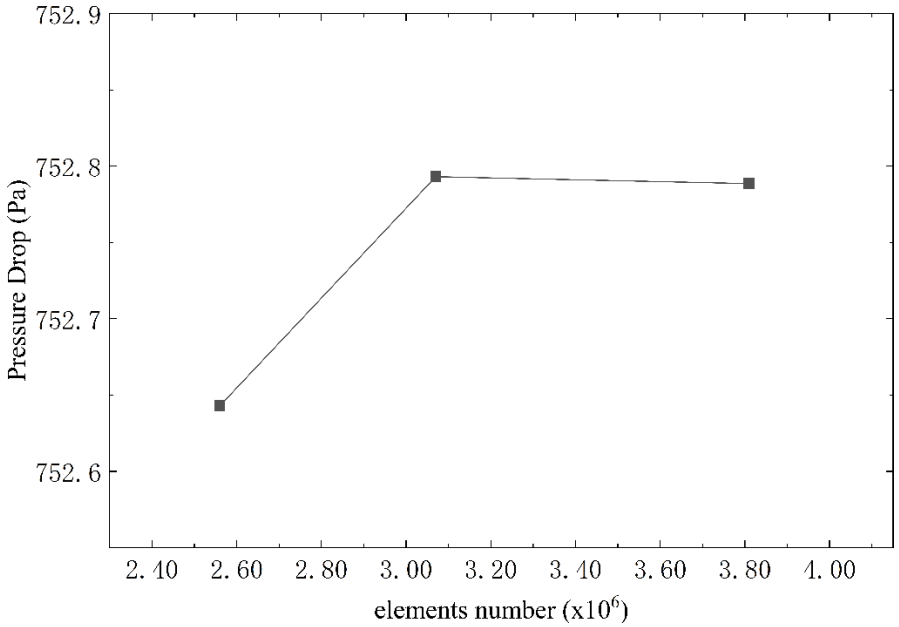


Figure 5 – Grid independence verification

3.3 Turbulence Model Validation

To further elucidate the intricate three-dimensional flow physics and localized transport phenomena within the cooling channels, steady-state numerical simulations were executed using a commercial finite-volume solver. The computational domains for all four investigated configurations—namely the baseline latticework channel, the impingement-zone slotted structure, the turning-zone slotted structure, and the simultaneous dual-slotted structure—were established to exactly replicate the geometric characteristics of the physical experimental models.

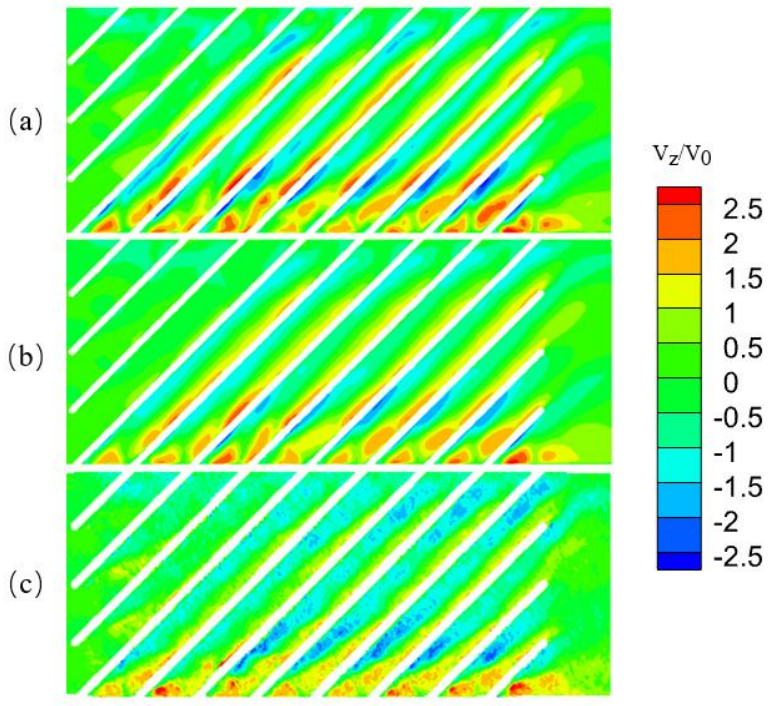


Figure 6 – Turbulence model validation against experimental data based on z-directional velocity contours at z/H = 0.75: (a) SST k-ω, (b) Realizable k-ε, and (c) MRV.

To ensure high-fidelity benchmarking, the boundary conditions implemented in the numerical solver were prescribed to perfectly mirror the experimental parameters. At the channel inlet, a uniform velocity profile corresponding to a Reynolds number of Re = 10,000 was imposed, based on a characteristic length (hydraulic diameter) of D_h = 0.04 m. The inlet turbulence intensity was set at 4.4% to closely emulate the upstream flow baseline of the experimental setup. A pressure outlet condition with zero gauge pressure was applied at the channel exit, and all solid boundaries were defined as adiabatic, no-slip walls.

Given the highly complex, three-dimensional nature of the flow inside the slotted latticework channels—which is characterized by strong flow separation, high-speed jet impingement, and sharp turning vortices—the selection of an appropriate turbulence model is paramount for securing accurate predictions. For this purpose, two widely adopted eddy-viscosity models were rigorously evaluated against the experimental full-field data: the SST k-ω model and the Realizable k-ε model combined with Enhanced Wall Treatment.

Figure 6 illustrates the comparative results of the z-directional velocity distribution contours at a representative spanwise plane of z/H = 0.75, where Fig. 6(a) represents the numerical prediction from the SST k-ω model, Fig. 6(b) displays the numerical prediction from the Realizable k-ε model, and Fig. 6(c) shows the full-field velocity data captured via the MRV experiment.

A detailed qualitative and quantitative comparison reveals that both numerical models are capable of capturing the global topological features of the flow, such as the high-velocity jet cores within the sub-channels and the low-speed wake regions downstream of the crossing ribs. However, distinct discrepancies arise in predicting the localized shear layers and peak velocity magnitudes. The SST k-ω model (Fig. 6(a)) tends to overpredict the turbulent momentum diffusion across the mixing layers, which consequently leads to an underestimation of the core velocity magnitude within the turning zone compared to the experimental benchmark.

In contrast, the Realizable k-ε model with Enhanced Wall Treatment (Fig. 6(b)) demonstrates exceptional agreement with the MRV experimental results (Fig. 6(c)). It precisely resolves the geometric contour of the high-velocity jet cores, the steep velocity gradients across the slot shear layers, and the asymmetric flow deflection induced by the interlocking rib layout. Consequently, due to its superior capability to faithfully capture both the spatial distribution and the precise magnitude of the three-dimensional velocity field, the Realizable k-ε model with Enhanced Wall Treatment was selected as the definitive turbulence model for all subsequent numerical investigations across the four structural configurations.

4. Results and Discussion

4.1 Effects of Slot Location on Swirl Flow in Sub-channels

Figure 7 illustrates the contours of the normalized z-directional velocity component at the sub-channel mid-span plane (z/H = 0.75) for the four investigated configurations. In the baseline configuration (Case 0, Fig. 7), the core region of the sub-channel exhibits a distinct antisymmetric velocity distribution, characterized by juxtaposed positive (red) and negative (blue) velocity zones. This bipolar velocity topology provides definitive flow-field evidence that the coolant advances downstream via a complex helical or swirling trajectory, which is a hallmark of the longitudinal vortex structures typically generated within interlocking latticework geometries. Concurrently, a pronounced velocity gradient is observed in close proximity to the sub-channel housing walls, signifying substantial fluid shear. As the main stream impinges upon and turns along the internal sidewalls, it undergoes a severe localized overturning motion, which serves as the primary hydrodynamic mechanism driving the generation and maintenance of these secondary swirling structures.

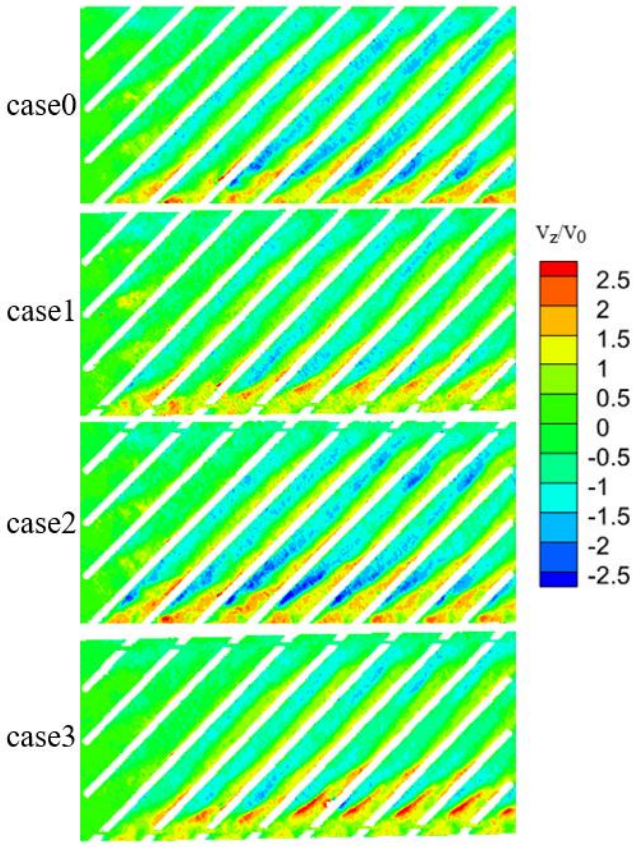


Figure 7 – Contours of normalized z-directional velocity component (V_z/V_0) at the sub-channel mid-span plane (z/H = 0.75) for different configurations

When a slot is incorporated into the impingement region (Case 1, Fig. 7), the local transport phenomena and vortex dynamics are significantly modified. The high-momentum leakage jet emanating from the impingement slot directly penetrates the sub-channel core flow, altering the baseline fluid trajectory. This cross-flowing leakage jet induces strong hydrodynamic interactions that partially disrupt and shear the coherent overturning vortex near the sidewall. Consequently, although the impingement jet successfully intensifies localized chaotic mixing and fluid renewal near the slot exit, it simultaneously suppresses the macro-scale swirl intensity within the sub-channel core, as manifested by the contraction and weakening of the antisymmetric z-velocity distribution.

Conversely, introducing the slot exclusively in the turning region (Case 2, Fig. 7) yields a drastically different flow response. The leakage flow passing through the turning slot exerts a negligible influence on the mixing characteristics at the overturning zone of the subsequent downstream sub-channel. However, it acts as a fluidic accelerator that tangentially feeds into the secondary flow, significantly amplifying the bulk rotational momentum of the core vortex. This targeted mass and momentum injection expands the high-velocity core regions within the swirling vortex structure, thereby markedly enhancing the sub-channel swirl intensity and sustaining a high velocity gradient near the heat transfer surfaces.

For the dual-slotted configuration (Case 3, Fig. 7), the resulting flow topology exhibits a synergistic amalgamation of the individual slot mechanisms, successfully inheriting the hydrodynamic advantages of both single-slotted designs. The "Both" configuration substantially augments localized fluid mixing and thermal rejuvenation at the sidewall turn via the impingement slot jet. Concurrently, the potential degradation of the macro-swirl intensity—originally caused by the impingement jet—is effectively mitigated by the favorable vortex reinforcement provided by the turning slot jet. This dual-slot strategy establishes an optimized balance between localized chaotic perturbation and global swirl preservation, maintaining highly energetic rotating structures alongside steep near-wall velocity gradients throughout the latticework channel network.

4.2 Improvement of Slotting on the Flow Dead Zones Near the Near-Endwall Plane

Figure 8 presents the contours of the normalized in-plane velocity magnitude within the xy-plane at the near-endwall region (z/H = 0.95) for the four investigated configurations. For the baseline unslotted configuration (Case 0, Fig. 8), a critical aerodynamic issue is observed along the peripheral sidewalls, characterized by extensive flow stagnation zones, commonly referred to as "flow dead zones." Within these regions, the boundary layer fluid suffers from a severe momentum deficit due to adversarial pressure gradients and geometry-induced flow separation. Notably, as the coolant progresses further into the downstream sub-channels, such as C7 and C8, this flow blockage exhibits a cumulative effect, deteriorating progressively. The persistent low-velocity stagnation zones in C7 and C8 provide clear evidence that the fluid becomes trapped within localized, low-energy recirculation vortices. This phenomenon drastically reduces effective flow capacity and impairs localized convective heat transfer due to the lack of fluid replenishment.

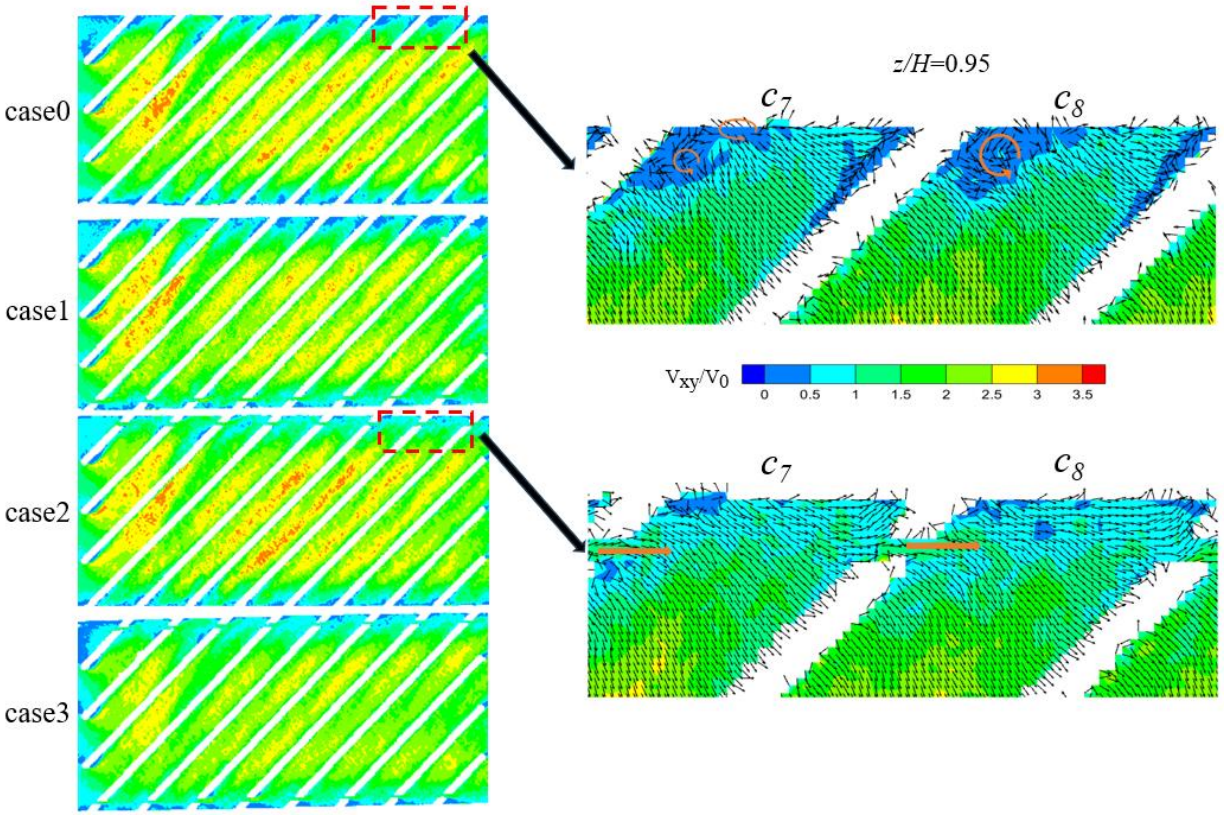


Figure 8 – Contours of normalized in-plane velocity magnitude within the xy-plane at the near-endwall region (z/H = 0.95) for different configurations

The implementation of slots fundamentally shifts the near-endwall vortex topology by establishing a continuous, self-governing purging mechanism. Regardless of the slot location, the geometric modification acts through a dual aerodynamic intervention: localized fluid aspiration (suction effect) at its upstream entrance and high-momentum jet emission (blowing effect) at its downstream exit. At the slot inlet, the local negative pressure gradient draws in the low-momentum boundary layer fluid, effectively thinning the blockaded fluid layer. Concurrently, the leakage jet discharging from the slot exit produces a powerful sweeping and flushing mechanism that directly strikes the core of the stagnant vortices. This combined action effectively destabilizes, disrupts, and subsequently reconstructs the trapped recirculation structures, preventing the formation of large-scale stagnant flow topologies.

Consequently, the prominent low-velocity stagnation zones previously observed in sub-channels C7 and C8 under the baseline case are successfully streamlined, dissipated, and re-energized across all slotted configuration. In the impingement-slotted channel (Case 1, Fig. 8), the purging effect is highly pronounced around the nominal impact zone, whereas the turning-slotted channel (Case 2, Fig. 8) significantly enhances fluid momentum along the turning periphery, straightening the recirculating paths. For the dual-slotted configuration (Case 3, Fig. 8), this aerodynamic flushing

mechanism reaches its maximum efficacy. The combination of suction and blowing from both slots ensures that the low-momentum vortices are thoroughly broken up and integrated into the high-velocity mainstream. This dual-slot strategy effectively recovers the available flow passage area, mitigates cumulative downstream flow blockage, and substantially reduces aerodynamic dead zones near the endwall surface.

4.3 Local Flow Topology and Jet Interactions at the Slotted Cross-Section

Figure 9 displays the contours of the normalized velocity magnitude at the longitudinal slot cut-plane (y/W = 0.4375), specifically capturing the localized flow behavior within sub-channels c4 and c5 across the four investigated configurations. In the baseline unslotted configuration (Case 0, Fig. 9), a prominent wake recirculation bubble, or low-velocity stagnation zone, forms immediately downstream of the sidewall ribs due to geometry-induced flow separation. Concurrently, as the coolant transitions from one sub-channel into the interlocking adjacent sub-channel across the rib boundary, the fluid undergoes severe localized overturning and convective acceleration. This dynamic process manifests as a distinct high-speed region situated near the channel sidewall, establishing a high-shear layer that characterizes the baseline inter-channel transport.

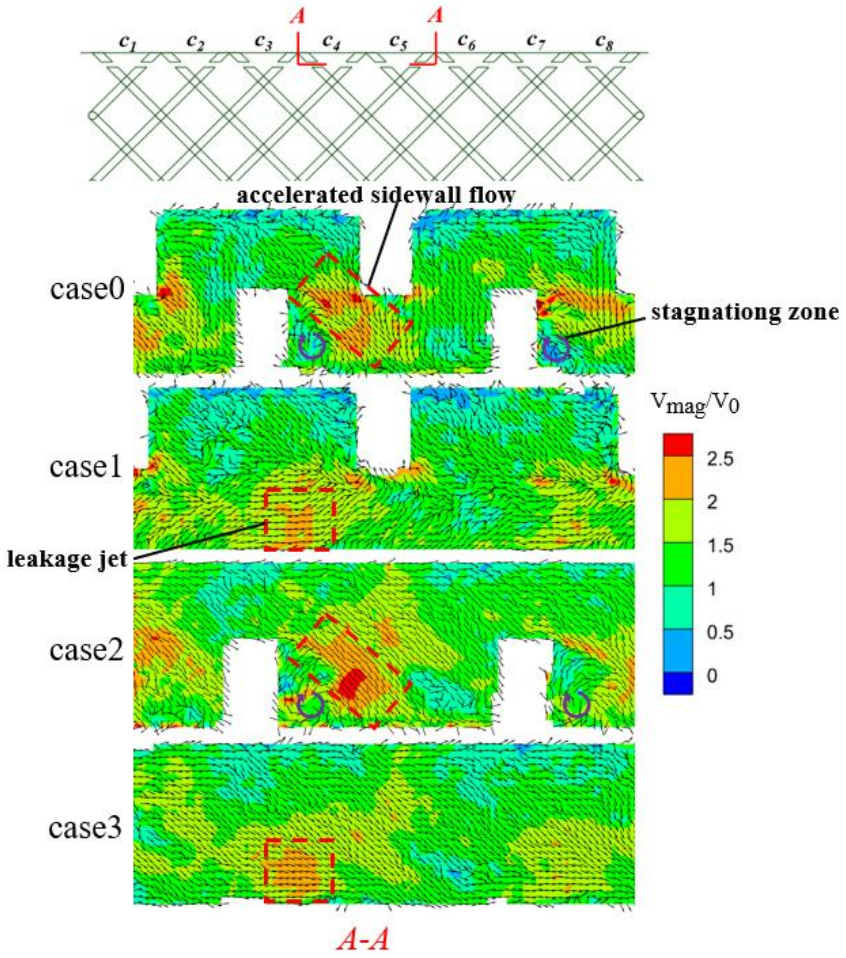


Figure 9 – Contours of normalized velocity magnitude at the slot cut-plane (y/W = 0.4375) within sub-channels c4 and c5 for different configurations

When the slot is introduced exclusively in the impingement region (Case 1, Fig. 9), this flow topology is radically altered. The conventional sidewall-directed overturning acceleration zone is replaced by an energetic, high-momentum leakage jet emerging directly from the slot exit. This newly developed impingement jet directly penetrates the wake region of the upstream rib, providing substantial kinetic energy that actively flushes and re-energizes the low-velocity stagnation zone. Consequently, the scale of the dead flow region within the impingement zone is significantly minimized, and local fluid rejuvenation is markedly enhanced.

For the turning-region slotted configuration (Case 2, Fig. 9), the flow remediation mechanism is decoupled from the upstream detachment zone. The introduction of the turning slot yields negligible improvements to the primary low-speed stagnation bubble formed behind the sidewall rib. Instead, its fluidic intervention is confined further downstream, where it successfully accelerates and re-energizes the low-velocity boundary layer fluid adjacent to the endwall within the turning zone. This indicates that while the turning slot enhances localized boundary layer flushing near the channel transitions, it lacks the hydrodynamics needed to disrupt the upstream separation bubble.
In the dual-slotted configuration (Case 3, Fig. 9), a comprehensive optimization of the local flow topology is achieved, successfully mitigating the low-velocity deficits near both endwall bounding regions. The fluid experiences highly intensive chaotic mixing and shear layer interaction at the interlocking slotted junctions, which promotes uniform momentum exchange. Notably, within this dual-slot framework, the high-velocity accelerated jet remains highly dominant and concentrated behind the impingement slot, maintaining its strong localized flushing capability. This collaborative slot layout ensures that the channel benefits from both the macro-scale separation suppression triggered by the impingement jet and the localized near-wall sweeping provided by the turning slot.

4.4 Effects of Slotting on Heat Transfer

Figure 10 illustrates the endwall Nusselt number contours at Re = 10000. For the baseline Case 0 high-Nu bands are concentrated at the sidewall fluid overturning locations, juxtaposed against low-heat-transfer zones governed by the rib wake recirculation bubbles. For Case 1, the impingement slot jet slightly dampens the fluid overturning intensity, causing a minor reduction in peak Nu, but successfully purges the low-velocity wake stagnation zones to limit low-heat-transfer area expansion. In Case 2, the turning slot induces intense fluidic mixing during the turning phase, producing localized high-Nu patches immediately downstream of the junctures; however, it fails to remediate the upstream rib wake separation, leading to downstream thermal degradation and enlarged low-Nu zones (blue regions). In contrast, the dual-slotted configuration Case 3 demonstrates superior thermal uniformity. The synergistic activation of upstream suction and downstream blowing systematically minimizes the low-Nu footprints by continuously re-energizing the persistent stagnation zones.

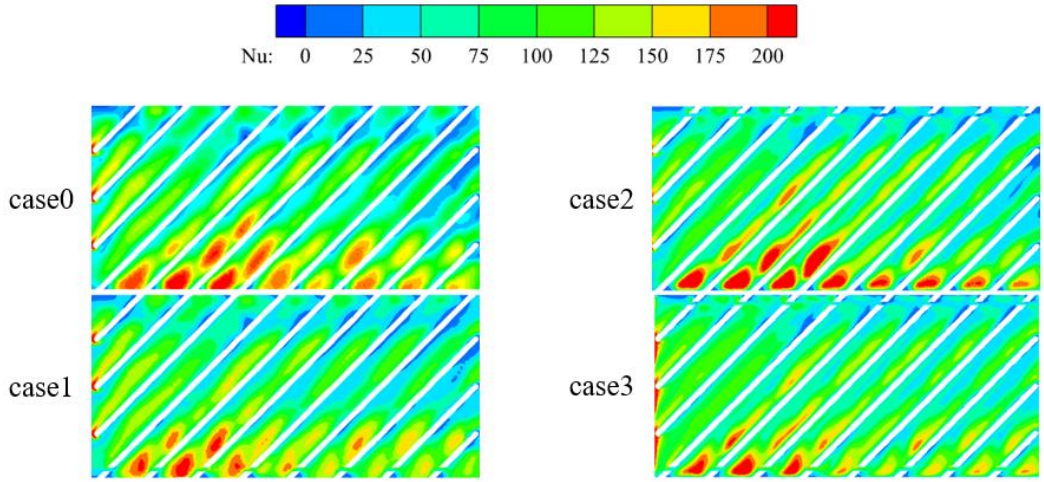


Figure 10 – Contours of Nusselt number (Nu) distribution on the endwall at Re = 10000 for different configurations

Figure 11 delineates the variations of friction factor ratio (f/f_0) and thermal performance factor (TPF) from Re = 10000 to 25000. Case 3 consistently exhibits a significantly lower f/f0 than Case 0 across all flow rates, primarily because the dual-slot configuration suppresses large-scale separations and recovers the effective passage area. Consequently, Case 3 delivers a superior TPF that increases monotonically with rising Re, highlighting its exceptional aerothermal viability under high-velocity

conditions. Conversely, Case 0 displays a parabolic TPF trajectory that peaks and subsequently deteriorates beyond Re = 20000. This degradation underscores a critical aerodynamic limitation of the baseline channel: since pressure drop scales quadratically with velocity, the parasitic friction penalty outpaces convective heat transfer gains at elevated Re without the flow-relief mechanisms provided by the dual slots.

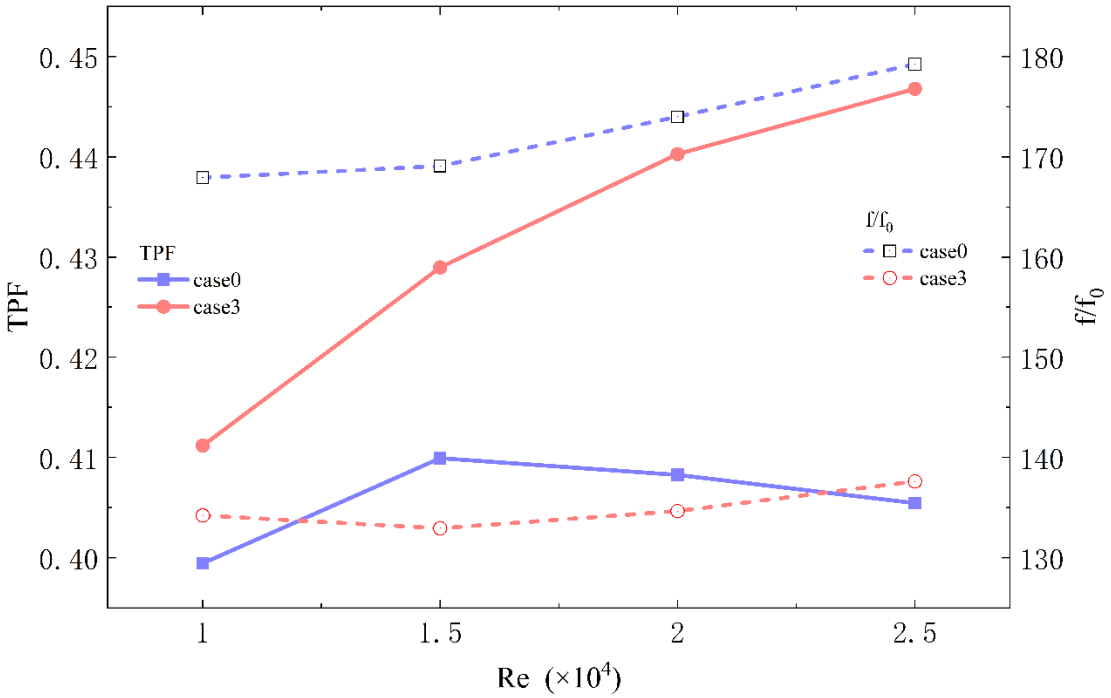


Figure 11 – Variations of friction factor ratio (f/f_0) and thermal performance factor (TPF) as a function of Reynolds number (Re) for Case 0 and Case 3

5. Conclusions

(1) The turning slot acts as a fluidic accelerator that significantly amplifies the core vortex rotational momentum, whereas the impingement slot intensifies local chaotic mixing at the expense of sub-channel macro-swirl intensity.

(2) The introduction of slots establishes a self-governing suction-and-blowing mechanism that effectively thins the boundary layer and purges the cumulative downstream near-endwall flow stagnation zones.

(3) The dual-slotted configuration (Case 3) successfully achieves a comprehensive aerodynamic optimization by suppressing large-scale flow separations and restoring the effective passage area.

(4) Case 3 consistently reduces the global pressure drop penalty across all flow rates, delivering a superior thermal performance factor that increases monotonically from Re = 10,000 to 25,000.

6. Contact Author Email Address

mailto: jyx1207@stu.xjtu.edu.cn; wjmxjtu@xjtu.edu.cn*

References

[1] Han, J. C., Dutta, S., & Ekkad, S. (2012). *Gas turbine heat transfer and cooling technology*. CRC press.

[2] Armstrong J, Winstanley D. A review of staggered array pin fin heat transfer for turbine cooling applications[J]. 1988.

[3] Bunker, R. S. (2004, January). Latticework (vortex) cooling effectiveness: Part 1—stationary channel experiments. In *Turbo Expo: Power for Land, Sea, and Air* (Vol. 41685, pp. 909-918).

[4] Saha, K., Acharya, S., & Nakamata, C. (2013). Heat transfer enhancement and thermal performance of lattice structures for internal cooling of airfoil trailing edges. *Journal of Thermal Science and Engineering Applications*, *5*(1), 011001.

[5] Tsuru, T., Ishida, K., Fujita, J., & Takeishi, K. (2019). Three-dimensional visualization of flow characteristics using a magnetic resonance imaging in a lattice cooling channel. *Journal of Turbomachinery*, *141*(6), 061003.

[6] Acharya, S., Zhou, F., Lagrone, J., Mahmood, G., & Bunker, R. S. (2005). Latticework (Vortex) cooling effectiveness: rotating channel experiments.

[7] Saha, K. (2012). *Turbine Blade Internal Cooling: Trailing Edge, Coolant-Passage Entry, Bend Effect and Improvement in Thermal Performance*. Louisiana State University and Agricultural & Mechanical College..

[8] Hagari, T., & Ishida, K. (2013, June). Numerical investigation on flow and heat transfer in a lattice (matrix) cooling channel. In *Turbo Expo: Power for Land, Sea, and Air* (Vol. 55140, p. V03AT12A040). American Society of Mechanical Engineers.

[9] Ramireddy, S. R., Gurusiddappa, S. P., Kesavan, V., & Kumar, S. K. (2014, December). Computational study of flow and heat transfer in matrix cooling channels. In *Gas Turbine India Conference* (Vol. 49644, p. V001T04A007). American Society of Mechanical Engineers.

[10] Choi, S. M., Bang, M., Kim, S. Y., Lee, H., Joo, W. G., & Cho, H. H. (2017). Numerical simulation of effect of various rib configurations on enhancing heat transfer of matrix cooling channel. *World Acad. Sci., Eng. Technol., Int. J. Mech. Mechatronics Eng.*, *11*(12), 1906-1910.

[11] Du, W., Luo, L., Wang, S., Liu, J., & Sunden, B. (2019). Effect of the broken rib locations on the heat transfer and fluid flow in a rotating latticework duct. *Journal of Heat Transfer*, *141*(10), 102102.

[12] Adrian, R. J. (2005). Twenty years of particle image velocimetry. *Experiments in fluids*, *39*(2), 159-169.

[13] Lauga, E., Brenner, M., & Stone, H. (2007). Springer handbook of experimental fluid mechanics.

[14] Jakirlić, S., Jester-Zürker, R., & Tropea, C. (2001). A novel near-wall turbulence model applied to separated flows. *Physics of Fluids*, 13(12), 3784-3794.

[15] Versteeg, H. K., & Malalasekera, W. (2007). *An Introduction to Computational Fluid Dynamics: The Finite Volume Method* (2nd ed.). Pearson Education.

[16] Elkins, C. J., & Alley, M. T. (2007). Magnetic resonance velocimetry: applications of magnetic resonance imaging in the measurement of fluid motion. *Experiments in Fluids*, 43(6), 823-858.

[17] Elkins, C. J., Markl, M., Pelc, N., & Eaton, J. K. (2003). Magnetic resonance velocimetry: a new tool for the investigation of complex flows. *Experiments in Fluids*, 34(1), 1-12.

[18] Elkins, C. J., Alley, M. T., Saetran, L., & Eaton, J. K. (2009). Three-dimensional turbulent flow measurements in a complex geometry using magnetic resonance velocimetry. *Experiments in Fluids*, 46(6), 1007-1018.

[19] Benson, M. J., Elkins, C. J., Mobley, P. D., et al. (2010). Three-component velocity field measurements in a film cooling flow using magnetic resonance velocimetry. *Journal of Turbomachinery*, 133(3), 031004.

[20] Duan, Y., et al. (2021). Experimental investigation of flow and heat transfer in a double-wall cooling structure using magnetic resonance velocimetry. *International Journal of Heat and Mass Transfer*, 178, 121625.

[21] Zhang, Y., et al. (2022). Validation of CFD models for double-wall cooling using magnetic resonance velocimetry data. *Applied Thermal Engineering*, 203, 117932.

[22] W. Jin, J. M. Wu, N. Jia, J. Lei, W. T. Ji and G. N. Xie, "Effect of shape and distribution of pin-fins on the flow and heat transfer characteristics in the rectangular cooling channel," Int. J. Therm. Sci., vol. 161, pp. 106758, 2021.

Copyright Statement

The authors confirm that they, and/or their company or organization, hold copyright on all of the original material included in this paper. The authors also confirm that they have obtained permission, from the copyright holder of any third party material included in this paper, to publish it as part of their paper. The authors confirm that they give permission, or have obtained permission from the copyright holder of this paper, for the publication and distribution of this paper as part of the ICAS proceedings or as individual off-prints from the proceedings.